A Measurement of the Proton g_2 Structure Function at Intermediate Q^2

(A submission to Jefferson Lab PAC-51)

Executive Summary

Jefferson Lab has been the premier facility to measure the nucleon spin-dependent structure functions. These functions are necessary for a complete picture of the nucleon's composite nature, and higher moments of these quantities have been used to test QCD sum rules, Lattice QCD and effective field theory treatments of QCD. As noted in the Department of Energy 2013 Comparative Review [1], *"Measurement of the nucleon polarized structure functions g_1 and g_2 over an enlarged range of Bjorken x, allowing tests of both chiral perturbation theory and perturbative QCD"* allows a 'particularly noteworthy' opportunity for future research.

In the past decade, the structure functions $g^n_{1,2}$ and g^p_1 have been precisely mapped in the resonance region, but data for the g^p_2 structure function is still relatively sparse, due largely to the significant technical challenges associated with operating a transversely polarized solid target. The transverse data measured to date provides strong motivation for further measurements. Surprising negative results were found for the proton's d_2 matrix element [2], and recently, measurements of the proton's longitudinal-transverse generalized polarizability [3] δ_{LT} revealed that two state of the art effective field theory treatments are still in tension with each other. The g^p_2 contribution to calculations of muonic hydrogen hyperfine splitting is dominated by measurments at low and intermediate Q^2. And finally, the satisfaction of the Burkhardt-Cottingham Sum Rule is still an open question; a three sigma deviation from the Burkhardt-Cottingham sum rule was found at large Q^2 for the proton, while it is satisfied for the neutron at low Q^2. Clearly, the situation would benefit from a more complete g^p_2 data set.

To this end, we propose to measure the polarized cross section difference $\Delta\sigma_\perp$ in order to access g^p_2 in the resonance region in the range $0.22 < Q^2 < 3.6$ GeV^2. We request 18 days of 4.4 GeV and 8.8 GeV polarized beam in Hall C, incident on the transversely polarized solid NH_3 target and a local low power beam dump. The existing 2 cm chicane used to bring the beam into the hall will be sufficient to deliver the beam on target before being spent on a local low power beam dump [4].

The data collected will be used to extract the higher moment $d^p_2(Q^2)$ matrix element, test the Burkhardt-Cottingham sum rule and evaluate the spin polarizability term of muonic hyperfine splitting in the range $0.27 < Q^2 < 1.2$ GeV^2 where no g^p_2 data currently exists. Additionally, data in the region $2.2 < Q^2 < 3.6$ GeV^2 will be used to further investigate the intriguing isospin independence of d^p_2 that was found by the SANE[2] experiment. Evaluation of these moments in the transition region is important for comparison to theory to fully understand the transition from perturbative QCD to non-perturbative QCD. In particular, Lattice QCD(LQCD) theorists expect to soon produce 4-point function calculations [5], which will enable direct theoretical predictions of the above moments in this regime. The higher Q^2 data requested by this proposal will also be used for a direct comparison to traditional 3-point function calculations of LQCD.

The Jefferson Lab g2p2 Collaboration

Anchit Arora, Elena Long, Michael McLellan,
David Ruth[†‡], **Nathaly Santiesteban**[†], **Karl Slifer**[†],
Nicholas Muche, Zoe Wolters, Allison Zec
University of New Hampshire, Durham, NH 03861

Alexandre Camsonne, **Jian-Ping Chen**[†], Silviu Covrig Dusa,
Alexandre Deur, Dave Gaskell, Mark Jones, Dave Mack
Thomas Jefferson National Accelerator Facility, Newport News, VA 23606

Whitney Armstrong, Sylvester Joosten, Zein-Eddine Meziani, Chao Peng
Argonne National Laboratory, Lemont, IL 60439

Hamza Ataç, Nikos Sparveris
Temple University, Philadelphia, PA 19122

Sebastian Kuhn, Pushpa Pandey
Old Dominion University, Norfolk, VA 23529

Garth Huber
University of Regina, Regina, SK S4S0A2, Canada.

Pete Markowitz
Florida International University, Miami, FL 33199

Arun Tadepalli
Rutgers University, New Brunswick, NJ 08901

Michael Nycz, Oscar Rondon-Aramayo, Jixie Zhang
University of Virginia, Charlottesville, VA 22904

Darko Androic
University of Zagreb, Faculty of Science, Croatia

Axel Schmidt
George Washington University, Washington, DC 20052

Simon Širca
Faculty of Mathematics and Physics, University of Ljubljana, Slovenia

[†]Spokesperson
[‡]Contact person: David Ruth, david.ruth@unh.edu

Contents

1 Introduction

There's been a strong commitment at JLab to extract the spin structure functions g_1^n, g_2^n and g_1^p and their moments over a wide kinematic range [6, 7, 8, 9, 10, 11, 12, 13, 14, 15, 3]. These moments have proven to be powerful tools to test QCD sum rules and examine the transition from the incoherent parton description of the nucleon to the more complex coherent properties of the nucleon. After a twenty year program, the g_2^p structure function remains mostly unmeasured, despite the coverage obtained by the SANE [16], RSS [7] and E08-027 [3] collaborations. These previous experiments have not yet explored a large region at moderate Q^2; This is surprising since the remaining region is rich with scientific motivation, and relatively speaking, this region is easier to access experimentally. Compared to previous efforts the scattering rates will be higher than those measured in RSS and SANE. And there is no need for a Septa magnet as was needed for E08-027. It is the rare case of the 'low hanging fruit' on the structure function tree remaining long after the more difficult branches have been accessed.

This proposal aims to fill the gap in our knowledge of the proton spin structure by performing a high precision measurement of g_2^p in the range $0.22 < Q^2 < 3.6$ GeV^2. The data will be used to extract the $d_2^p(Q^2)$ matrix element, test the Burkhardt-Cottingham sum rule and evaluate the spin polarizability term of muonic hyperfine splitting in the range where no g_2^p data currently exists. Where possible, we expect to compare to predictions of Lattice QCD, including upcoming calculations in the transition region [5].

2 Theoretical Background

We introduce here the g_2 spin structure function and the motivation for measuring this quantity. The g_2 structure function is a quantity which can be derived in spin-$\frac{1}{2}$ systems which, along with its twin g_1, provides information on how the nucleon's spin structure varies from point-like behavior at constant Q^2. Further, these quantities are extremely important because it is possible to construct integrals, also known as sum rules or moments, of these quantities which can be derived directly from theoretical predictions. At low Q^2, this provides a means to test effective theories such as Chiral Perturbation Theory, but in the intermediate Q^2 range of this proposal, they can instead be used to test upcoming predictions of Lattice QCD [5], which may help to bridge the gap between perturbative QCD and the realm of effective theories.

2.1 The g_2 Structure Function

If we define $q_f(x)dx$ { and $\overline{q}_f(x)dx$ } as the expectation value for the number of quarks { and anti-quarks } of flavor f in the hadron whose momentum fraction lies in the interval $[x, x+dx]$, then in the parton model it can be shown that:

$$F_1(x) = \frac{1}{2}\sum_f z_f^2 \left(q_f(x) + \overline{q}_f(x)\right) \tag{1}$$

and

$$g_1(x) = \frac{1}{2}\sum_f z_f^2 \left(q_f(x) - \overline{q}_f(x)\right) \tag{2}$$

where the quark charge z_f enters due to the fact that the cross section is proportional to the squared charge of the target. The Callan-Gross [17] relation shows that F_2 can be defined entirely in terms of F_1, but there is no such simple physical interpretation of g_2. This spin-dependent structure function is determined by the

x-dependence of the quarks' transverse momenta and the off-shellness, both of which are unknown in the parton model [18].

Ignoring quark mass effect of order $\mathcal{O}(m_q/\Lambda_{QCD})$, g_2 can be separated into leading and higher-twist components as:

$$g_2(x,Q^2) = g_2^{\mathtt{WW}}(x,Q^2) + \overline{g}_2(x,Q^2) \tag{3}$$

where

$$\overline{g}_2(x,Q^2) = -\int_x^1 \frac{\partial}{\partial y}\left[\frac{m_q}{M}\, h_T(y,Q^2) + \zeta(y,Q^2)\right]\frac{dy}{y} \tag{4}$$

To twist-3, there are three contributions to g_2:

1. $g_2^{\mathtt{WW}}$: The leading twist-2 term, which depends only on g_1.
2. h_T : Arises from the quark transverse polarization distribution. Also twist-2, this term is suppressed by the smallness of the quark mass.
3. ζ : The twist-3 part which arises from quark-gluon interactions.

The Wandzura–Wilczek [19] relation:

$$g_2^{\mathtt{WW}}(x,Q^2) = -g_1(x,Q^2) + \int_x^1 \frac{dy}{y} g_1(y,Q^2) \tag{5}$$

describes the leading twist part of the g_2 completely in terms of g_1. In reality, Eq. 5 is a good approximation only in the limit $Q^2 \to \infty$. At low Q^2 kinematics, g_2 exhibits strong deviations from leading twist behaviour as discussed in Sec. 3. This gives g_2 a unique sensitivity to higher twist, *i.e.* interaction-dependent effects in QCD [18].

2.2 Sum Rules and Moments

Sum rules involving the spin structure of the nucleon offer an important opportunity to study QCD. In recent years the Bjorken sum rule at large Q^2, and the Gerasimov-Drell-Hearn (GDH) sum rule [20] at $Q^2 = 0$, have attracted a concerted experimental and theoretical effort (see for example [21]). Another class of sum rules address the generalized GDH sum [22] and the spin polarizabilities [23]. These sum rules which are based on unsubtracted dispersion relations and the optical theorem relate the moments of the spin structure functions to real or virtual Compton amplitudes, which can be calculated theoretically.

Considering the forward spin-flip doubly-virtual Compton scattering (VVCS) amplitude g_{TT}, and assuming it has an appropriate convergence behavior at high energy, an unsubtracted dispersion relation leads to the following equation for g_{TT} [12, 23]:

$$\mathrm{Re}[g_{TT}(\nu,Q^2) - g_{TT}^{pole}(\nu,Q^2)] = (\frac{\nu}{2\pi^2})\mathcal{P}\int_{\nu_0}^{\infty} \frac{K(\nu',Q^2)\sigma_{TT}(\nu',Q^2)}{\nu'^2-\nu^2}d\nu', \tag{6}$$

where g_{TT}^{pole} is the nucleon pole (elastic) contribution, $\mathcal{P}$ denotes the principal value integral and K is the virtual photon flux factor. The lower limit of the integration ν_0 is the pion-production threshold on the nucleon. A low-energy expansion gives:

$$\mathrm{Re}[g_{TT}(\nu,Q^2) - g_{TT}^{pole}(\nu,Q^2)] = (\frac{2\alpha}{M^2})I_{TT}(Q^2)\nu + \gamma_0(Q^2)\nu^3 + O(\nu^5). \tag{7}$$

Combining Eqs. (1) and (2), the $O(\nu)$ term yields a sum rule for the generalized GDH integral [23, 22]:

$$\begin{aligned} I_{TT}(Q^2) &= \frac{M^2}{4\pi^2\alpha}\int_{\nu_0}^{\infty}\frac{K(\nu,Q^2)}{\nu}\frac{\sigma_{TT}}{\nu}d\nu \\ &= \frac{2M^2}{Q^2}\int_0^{x_0}\Big[g_1(x,Q^2)-\frac{4M^2}{Q^2}x^2g_2(x,Q^2)\Big]dx. \end{aligned} \tag{8}$$

The low-energy theorem relates I(0) to the anomalous magnetic moment of the nucleon, κ, and Eq. (8) becomes the original GDH sum rule [20]:

$$I(0)=\int_{\nu_0}^{\infty}\frac{\sigma_{1/2}(\nu)-\sigma_{3/2}(\nu)}{\nu}d\nu=-\frac{2\pi^2\alpha\kappa^2}{M^2}, \tag{9}$$

where $2\sigma_{TT}\equiv\sigma_{1/2}-\sigma_{3/2}$. The $O(\nu^3)$ term yields a sum rule for the generalized forward spin polarizability [23]:

$$\begin{aligned} \gamma_0(Q^2) &= (\frac{1}{2\pi^2})\int_{\nu_0}^{\infty}\frac{K(\nu,Q^2)}{\nu}\frac{\sigma_{TT}(\nu,Q^2)}{\nu^3}d\nu \\ &= \frac{16\alpha M^2}{Q^6}\int_0^{x_0}x^2\Big[g_1(x,Q^2)-\frac{4M^2}{Q^2}x^2g_2(x,Q^2)\Big]dx. \end{aligned} \tag{10}$$

Considering the longitudinal-transverse interference amplitude g_{LT}, the $O(\nu^2)$ term leads to the generalized longitudinal-transverse polarizability [23]:

$$\begin{aligned} \delta_{LT}(Q^2) &= (\frac{1}{2\pi^2})\int_{\nu_0}^{\infty}\frac{K(\nu,Q^2)}{\nu}\frac{\sigma_{LT}(\nu,Q^2)}{Q\nu^2}d\nu \\ &= \frac{16\alpha M^2}{Q^6}\int_0^{x_0}x^2\Big[g_1(x,Q^2)+g_2(x,Q^2)\Big]dx. \end{aligned} \tag{11}$$

Polarizabilities Sum Rule

Lensky et al. [24] report the following sum rule for the LT polarizability:

$$\delta_{LT}=-\gamma_{E1E1}+3M\alpha_{em}\Big[P'^{(M1,M1)1}(0)-P'^{(L1,L1)1}(0)\Big] \tag{12}$$

This sum rule can be re-expressed as

$$\begin{aligned} I_2^{(3)\prime}(0) &= \frac{M^2}{2}\{-\frac{1}{\alpha_{\rm em}}\left[\gamma_0+\gamma_{E1E1}\right] \\ &+ 3M\Big[P'^{(M1,M1)1}(0)-P'^{(L1,L1)1}(0)\Big]\} \end{aligned} \tag{13}$$

where the observable $I_2^{(3)}(Q^2)$ is defined through the third moment of the spin structure function g_2 as

$$I_2^{(3)}(Q^2) \equiv \frac{8M^4}{Q^4}\int_0^{x_0}dx\,x^2\,g_2\,(x,\,Q^2) \tag{14}$$

The right hand side of Eqs. 13 and 14 are all observables that can be measured in real compton scattering (RCS) and virtual compton scattering (VCS), so these two equations provide a model-independent and predictive relation among low-energy spin structure constants of the nucleon [24]

Large Q^2 Scaling

At large Q^2, the ratio of the two generalized polarizabilities is expected to demonstrate a scaling behaviour [23]:

$$\delta_{LT}(Q^2) \rightarrow \frac{1}{3}\gamma_0(Q^2) \tag{15}$$

Although this is expected to hold only as $Q^2 \rightarrow \infty$, the region at which this begins to manifest is still an open question, and may be as low as 0.9-1.0 GeV^2.

The Burkhardt-Cottingham Sum Rule

Alternatively, we can consider the covariant spin-dependent VVCS amplitudes S_1 and S_2, which are related to the spin-flip amplitudes g_{TT} and g_{LT}. The unsubtracted dispersion relations for S_2 and νS_2 lead to a super-convergence relation based on Regge asymptotics which is valid for all Q^2:

$$\int_0^1 g_2(x, Q^2)dx = 0, \tag{16}$$

where the integration includes the elastic peak. This sum rule was originally proposed by Burkhardt and Cottingham (BC) [25]. At first glance, it appears to be a trivial consequence of the $n = 1$ term of the operator product expansion (OPE) of Γ_2 (See for example [26]). But the expansion is valid only for $n \geq 3$. The OPE actually gives no information about the BC sum rule [18].

The validity of the BC sum rule depends on convergence of the integral, which would fail [27] for example, if g_2 exhibits non-Regge behaviour at low x, or exhibits a delta function singularity at $x = 0$. It is these criteria for a possible violation that have lead some authors to conclude [28] that "the B.C. integral is either zero or infinite".

Higher Moment $d_2(Q^2)$

At large Q^2, the d_2 matrix element is related to the color polarizabilities, which describe how the color electric and magnetic fields respond to the nucleon spin (see for example [29]). At lower momentum transfer, a moment identified with this matrix element, $\overline{d_2}(Q^2)$, provides a means to study the transition from perturbative to non-perturbative behaviour and to quantify higher twist effects via:

$$\overline{d_2}(Q^2) \;\; = \;\; 3\int_0^1 x^2 \left[g_2(x, Q^2) - g_2^{WW}(x, Q^2)\right] dx \tag{17}$$

The lowest twist component in d_2 is twist-3, although higher twists can also contribute at low Q^2. And although d_2 is a higher-twist OPE object, the definition holds for all Q^2. Then d_2 is just the x^2 moment of the difference between g_2 and g_2^{WW} even at low momentum transfer. It must vanish for $Q^2 \rightarrow 0$, and $Q^2 \rightarrow \infty$ but peaks around 1 GeV^2. In this sense, it represents a measure of QCD complexity and is of significant interest to map out d_2 over all Q^2.

Hyperfine Structure Contribution

The hyperfine structure of the hydrogen atom has been experimentally measured with extreme precision in atomic physics, but there are large uncertainties remaining in the theoretical approach. These are driven by a lack of understanding of the proton's internal structure, which contributes to the two-photon contribution to hyperfine splitting [30]:

$$E^{2\gamma}_{nS-hfs} = \frac{E_F}{n^3}\Big(\Delta_Z + \Delta_{recoil} + \Delta_{pol}\Big) \tag{18}$$

Here the Δ_{pol} term represents contributions from the proton's internal structure, split into two other contributions, Δ_1 and Δ_2:

$$\Delta_{pol} = \frac{\alpha m_e}{\pi g_p M_p}\Big(\Delta_1 + \Delta_2\Big) \tag{19}$$

The second of these can be written in terms of the g_2 structure function which this experiment aims to measure:

$$\Delta_2 = -24M_p^2 \int_0^\infty \frac{dQ^2}{Q^4} \int_0^{x_{th}} \tilde{\beta}_2(\tau) g_2(x, Q^2) dx \tag{20}$$

Where $\tilde{\beta}_2$ is a kinematic factor which depends on x and varies between electronic and muonic hydrogen with the mass of the lepton. Though much of the strength of this contribution is at lower Q^2 due to the strong $\frac{1}{Q^4}$ weighting of the integral, existing data and models expect a significant amount of strength remains in the region $0.22 < Q^2 < 1.0$ GeV^2, necessitating further measurement in this region for a complete understanding of atomic hyperfine structure.

3 Existing Data

The bulk of world g_2^p data comes from the SLAC E155x [31] experiment, and the Jefferson Lab SANE [16], RSS [7] and E08-027 [3] collaborations. SLAC experiment E155x [31] measured DIS g_2 for the proton and deuteron. The kinematic range was $0.02 \leq x \leq 0.8$ and $0.7 \leq Q^2 \leq 20$ GeV^2. The results (see Fig. 3) are consistent with the leading twist g_2^{WW} prediction, but with large error bars that don't exclude the possibility of higher twist effects. The resonance region at lower Q^2 was investigated by the RSS and the E08-027 collaborations at JLab. Fig. 2 shows proton g_2 data at $Q^2 \approx 1.3$ GeV^2 from RSS [7] compared to g_2^{WW}, the Simula model [32], Hall B model [33] and MAID [34].

Figs 1, 2 and 3 reveal that the dominant Delta resonance at $W = 1232$ MeV is positive for the two lowest Q^2 measurments (RSS, E08-027) before switching signs at the large Q^2 of E155x. The Burkhardt-Cottingham sum rule requires that the integration of g_2 over the entire x-range will sum to zero. In the large Q^2 SLAC data, we see that a large part of this cancellation occurs in the resonance region, while for the lower Q^2 data, a significant contribution to the integral must come from the unmeasured region at low x.

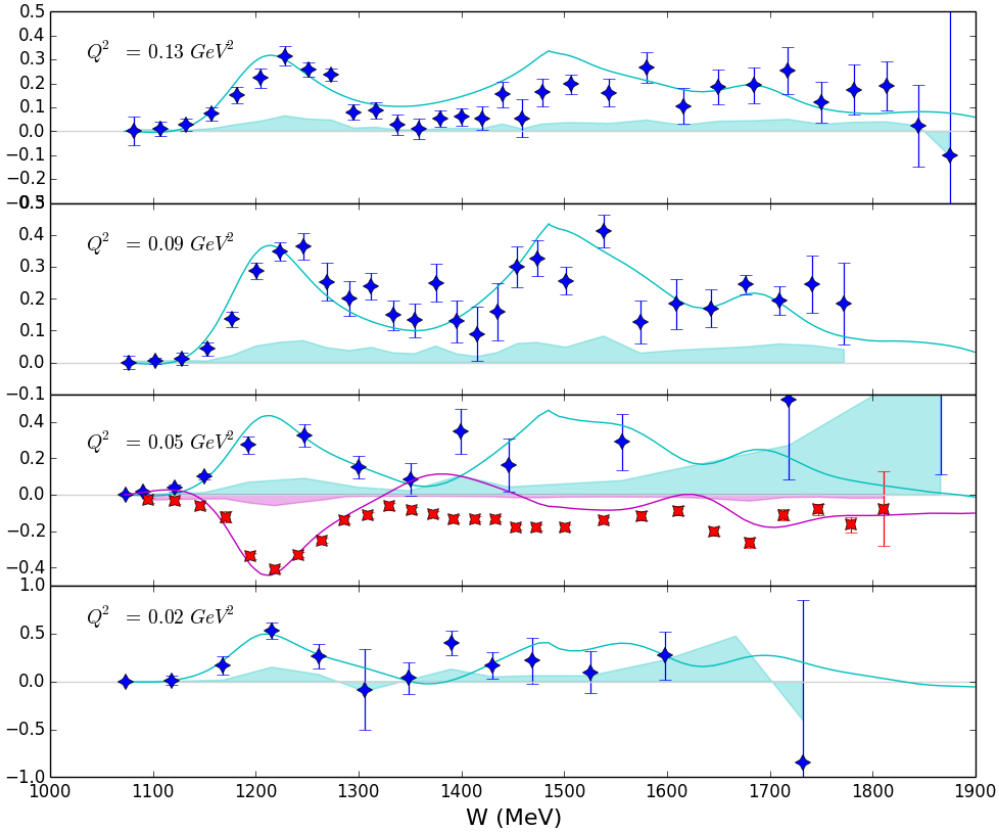

Figure 1: The proton spin structure functions of E08-027 [3]: g_1 (Red X ordinal stars) and g_2 (Blue cardinal Stars) as a function of invariant mass, W at constant Q^2. The error bars are statistical and the shaded region represents the scale of the systematic error.

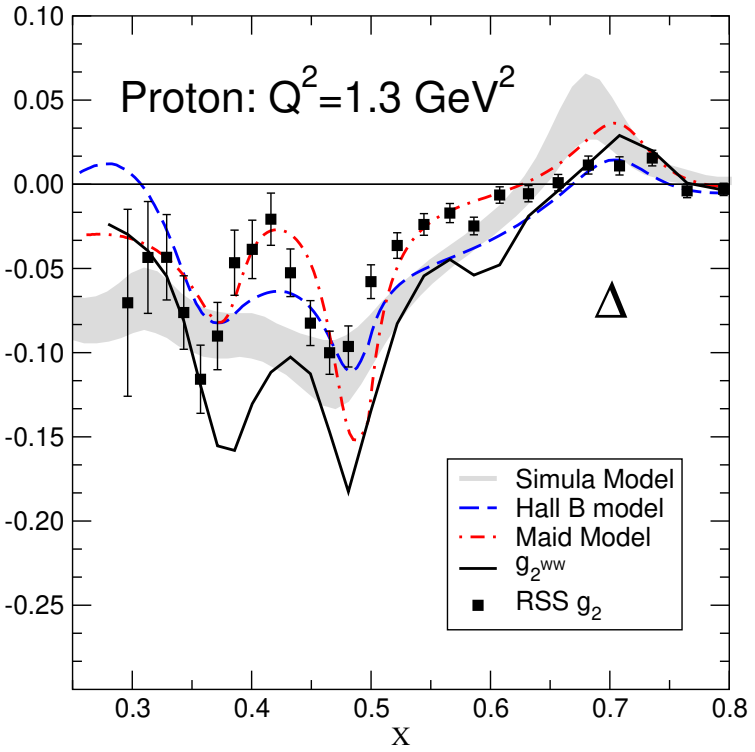

Figure 2: RSS experiment proton g_2 at $Q^2 \approx 1.3$ GeV^2 compared to g_2^{WW}, Simula model [32], Hall B model [33] and MAID [34]. Location of the $\Delta(1232)$ resonance indicated at large x.

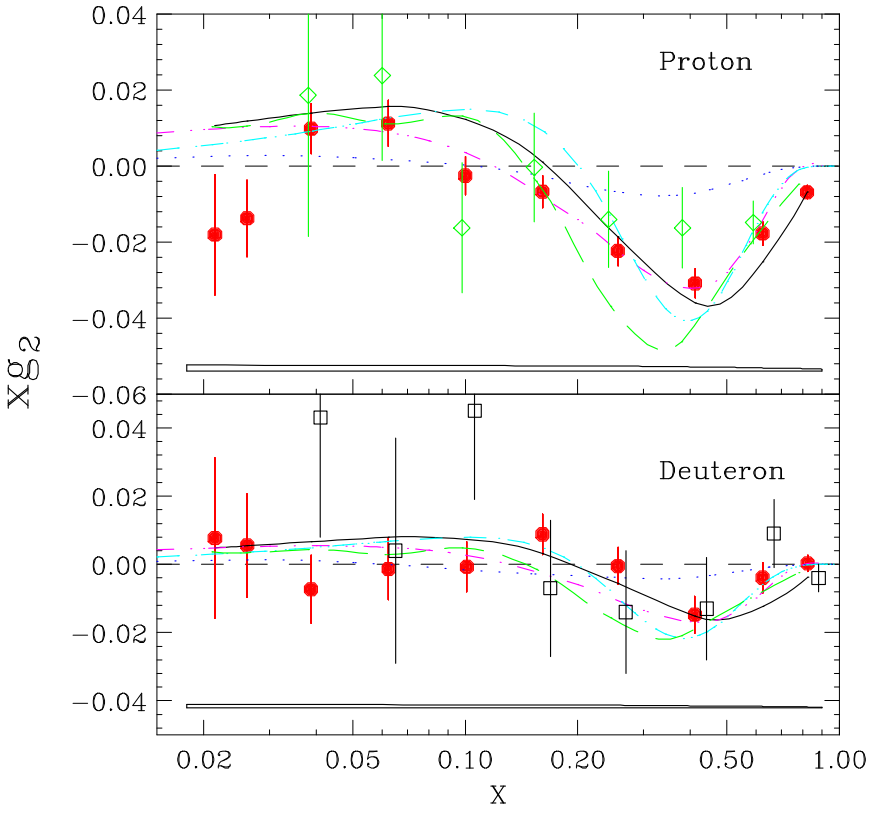

Figure 3: Q^2 averaged (0.8–8.2 GeV^2) xg_2 from E155x (solid circle), E143 (open diamond) and E155 (open square). Error bars are statistical. Also shown is g_2^{WW} (solid line) at the average Q^2 of E155x. Curves are the bag model calculations of Stratmann[35] (dash-dot) and Song[36] (dot) and the chiral soliton models of Weigel and Gamberg[37] (short dash) and Wakamatsu[38] (long dash). *Reproduced from [31].*

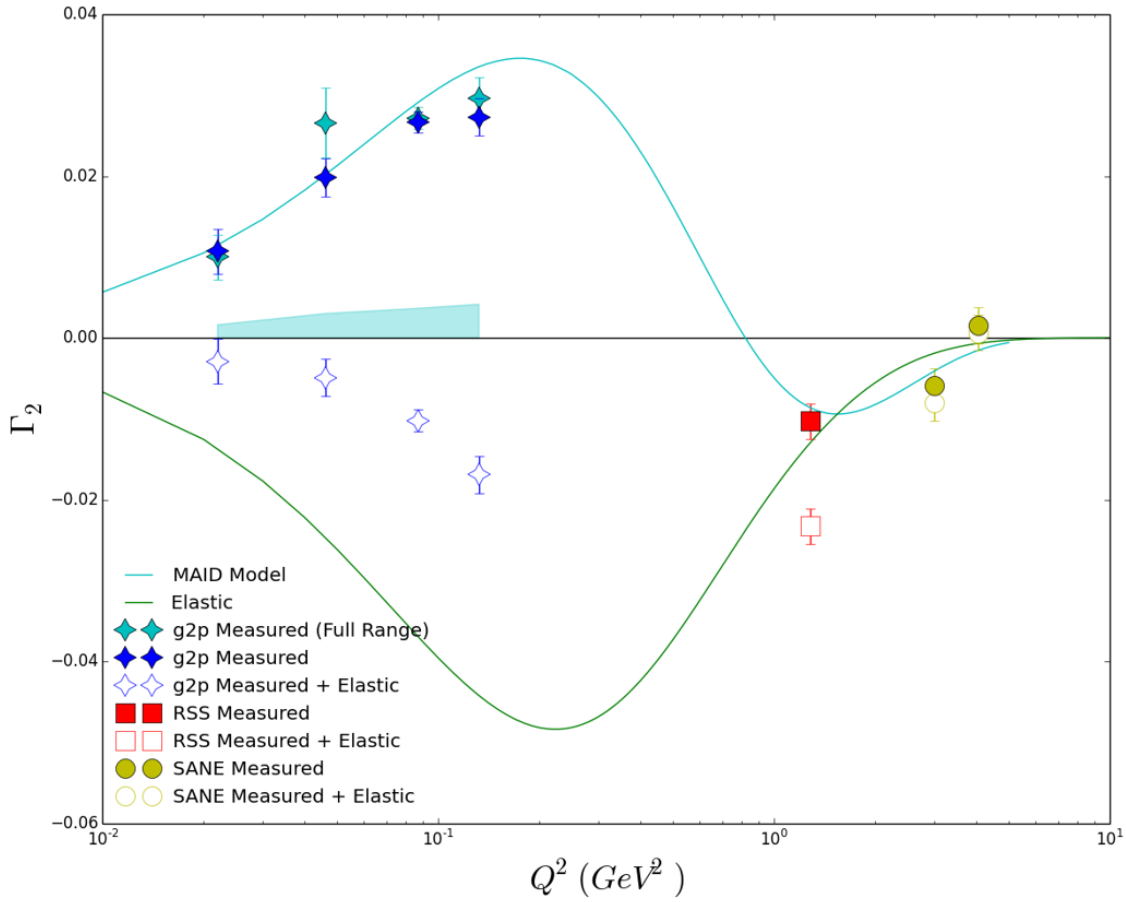

Figure 4: The Γ_2 moment. Light blue points represent an integral of the full measured region of E08-027, while dark blue points are limited to a maximum W of 1725. The MAID phenomenological model [34] is also run over this limited W range, as are the other experiments' results, to provide an even comparison. Results of RSS [7] are shown in red, and results of SANE [2] are shown in yellow. The open symbols represent the sum of the measured and elastic parts of the integral, excluding only the unmeasured high-W part.

3.1 The Burkhardt-Cottingham Sum Rule

Fig. 4 shows the Burkhardt-Cottingham integral $\Gamma_2(Q^2) = \int g_2 dx$ from pion threshold to $W = 2$ GeV. The capability to transversely polarize target allowed for the precise measurements of g_2 needed for the BC sum. The measured region is shown with solid circles, and the MAID estimate should be compared directly to these resonance region points. The total integral exhibits a striking cancellation of the inelastic (resonance+DIS) and elastic contributions, leading to an apparent satisfaction of the Burkhardt-Cottingham sum rule within uncertainties.

The SLAC E155x collaboration [39] previously reported a neutron result at high Q^2, which is consistent with zero but with a rather large error bar. On the other hand, the SLAC proton result deviated from the BC sum rule prediction by 3 standard deviations [40]. E155x covered the x-range $0.02 - 0.8$. The extended Q^2 coverage (0.8–8.2 GeV^2) was averaged to 5 GeV^2. For the unmeasured contribution as $x \to 0$, they assumed $g_2 = g_2^{WW}$. Also shown along are the results from RSS [7] which covered $W < 1.910$ MeV at

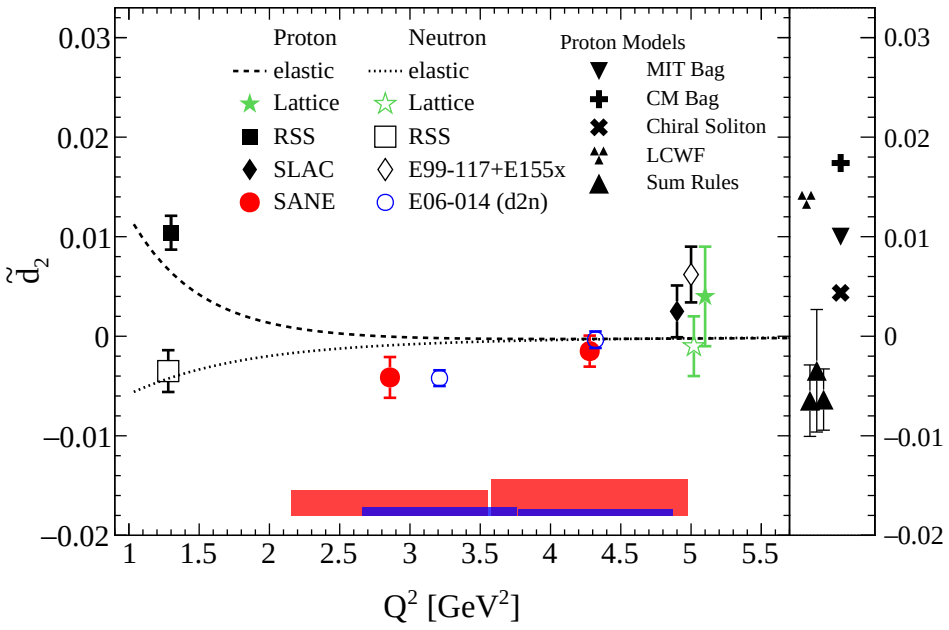

Figure 5: $\tilde{d}_2$ of the proton from SANE and recent neutron results [41]. Also shown are the lattice QCD results [42], previous proton (neutron) measurements with filled (open) symbols from SLAC [31], E99-117 and E155x [39], and RSS [43, 44] experiments. The dashed (dotted) lines show the elastic contribution for the proton (neutron). The panel on the right shows proton model calculations from QCD sum rules [45], the bag model [46], the Center-of-Mass (CM) bag model [36], the chiral soliton model [37], and light-cone wave functions (LCWF) [47].

$Q^2 \approx 1.3$ GeV^2. Open square represents the measured data, while the circular symbols include estimates of the unmeasured region (open) and the elastic contribution at $x = 1$. Inner (outer) error bars represent statistical (total) uncertainty. At this Q^2, the BC sum rule appears to be satisfied within the experimental error.

3.2 Higher Moment $d_2(Q^2)$

The Spin Asymmetries of the Nucleon Experiment (SANE) [2] measured g_2^p and the d_2^p matrix element for $0.3 < x < 0.8$, as shown in Fig. 5. The twist-3 matrix element, d_2^p, is proportional to an average color Lorentz force, and was extracted from the measured asymmetries at Q^2 values ranging from 2.0 to 6.0 GeV^2. The data surprisingly display the opposite sign compared to most quark models, including the lattice QCD result. The SANE data also has the opposite sign to the RSS and E08-027 measurements. Ref. [2] notes that when compared to the neutron data in the same Q^2 range their results suggest a flavor independent average color Lorentz force. The RSS and SANE points for this moment are calculated as a Nachtmann moment [7, 16], incorporating potentially large target mass corrections that are ignored in the Cornwall-Norton moment of 17.

Fig. 6 shows that the Q^2 evolution of the proton d_2 to lower Q^2. E155x [31] provides one point at

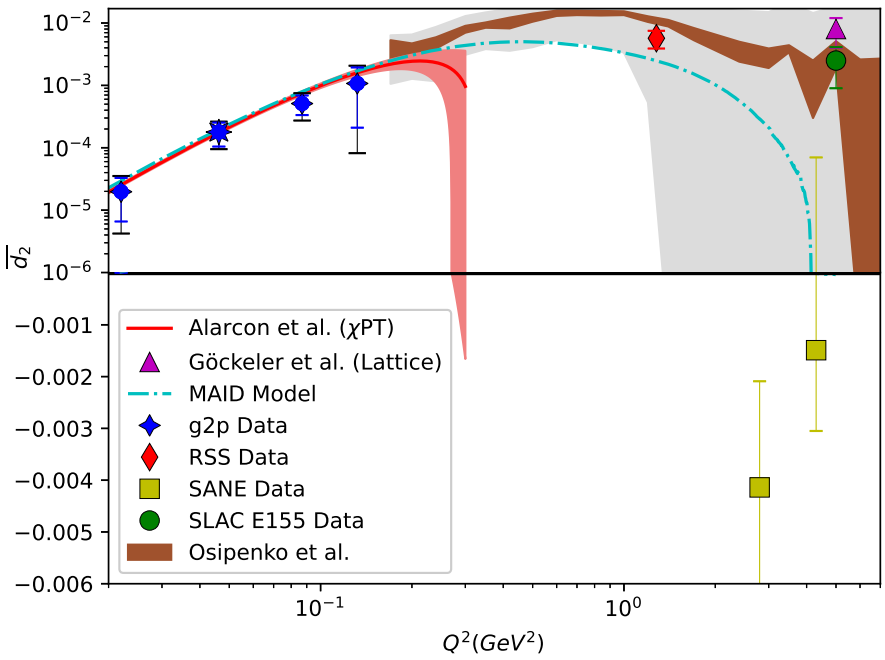

Figure 6: $\overline{d_2}$ for the proton as a function of Q^2, compared to existing data [7, 31, 2], the phenomenological models [34, 48], χPT calculations [49] and a Lattice QCD calculation [42]. The region above zero is shown on a log scale on the y axis to clearly show the comparison with the model, while the negative half of the plot is shown on a linear scale to allow the proper inclusion of the SANE [2] data. The statistical (total) uncertainty of our meausurement is represented with the inner (outer) error bars.

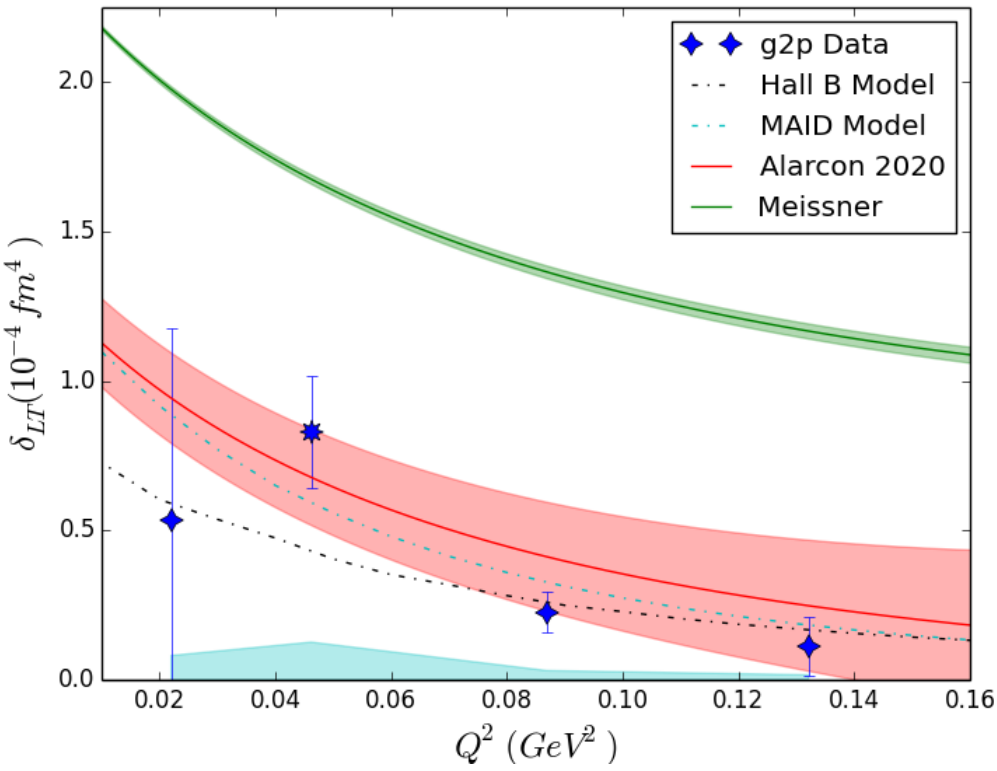

Figure 7: The generalized forward spin longitudinal-transverse spin polarizability for the proton as a function of Q^2, compared to existing world data,phenomenological models and χPT calculations. The δ_{LT} point indicated by an 8-pointed marker near $Q^2 = 0.45\ GeV^2$ includes both g_1 and g_2 from E94010 Data, while the other three points use the CLAS Model for the g_1 part of the integral.

an average Q^2 of 5.0 GeV^2 and RSS [7] measured d_2^p at $Q^2 \approx 1.3$ GeV^2. The large shaded area represents the global analysis of Osipenko et al. [48] using the existing g_1^p data [11] and the MAID [34] model. However, the MAID model disagrees strongly with the existing data, and the authors of [48] note that '*new experimental data on g_2 in the resonance region at different Q^2 values are clearly needed*'.

3.3 Spin Polarizability δ_{LT}

The nucleon polarizabilities are fundamental observables that characterize nucleon structure, and are related to integrals of the nucleon excitation spectrum. The electric and magnetic polarizabilities measure the nucleon's response to an external electromagnetic field. Because the polarizabilities can be linked to the forward Compton scattering amplitudes, real photon Compton scattering experiments [50] were performed to measure them. Another polarizability, associated with a spin-flip, is the forward spin polarizability γ_0. It has been measured in an experiment at MAMI (Mainz) [51] with a circularly polarized photon beam on a longitudinally polarized proton target.

The extension of these quantities to the case of virtual photon Compton scattering with finite four-momentum-squared, Q^2, leads to the concept of the generalized polarizabilities. See for example Ref. [24]. Generalized polarizabilities are related to the forward virtual Compton scattering (VCS) amplitudes and

the forward doubly-virtual Compton scattering (VVCS) amplitudes [21]. With this additional dependence on Q^2, the generalized polarizabilities provide a powerful tool to probe the nucleon structure covering the whole range from the partonic to the hadronic region. Some generalized polarizabilities data has recently become available for the first time: At MAMI, there is the real photon measurement of γ_0 for the proton [52], and the doubly polarized VCS experiment A1/01-00 [51] has been approved to run. At JLab an extraction of $\gamma_0^n(Q^2)$ and $\delta_{LT}^n(Q^2)$ was performed by E94010 [6], and the EG1b collaboration [33] has also released data for $\gamma_0^p(Q^2)$.

Since the generalized polarizabilities defined in Eqs. 10 and 11 have an extra $1/\nu^2$ weighting compared to the first moments, these integrals have only a small contribution from the large-ν region and converge quickly, which minimizes the uncertainty due to extrapolation. Measurements of the generalized spin polarizabilities are an important step in understanding the dynamics of QCD in the chiral perturbation region. At low Q^2, the generalized polarizabilities have been evaluated with next-to-leading order χPT calculations [53, 54]. One issue in these calculations is how to properly include the nucleon resonance contributions, especially the Δ resonance. As was pointed out in Refs. [53, 54], while γ_0 is sensitive to resonances, δ_{LT} is insensitive to the Δ resonance. It is expected that at large Q^2, the Q^6-weighted spin polarizabilities become independent of Q^2 (scaling) [23].

It is interesting to note that the deep-inelastic-scattering (DIS) Wandzura-Wilczek relation [19] leads to a relation between γ_0 and δ_{LT}:

$$\delta_{LT}(Q^2) \rightarrow \frac{1}{3}\gamma_0(Q^2) \quad \text{as} \quad Q^2 \rightarrow \infty. \tag{21}$$

which implies a sign change of one of the polarizabilities at finite Q^2.

4 Proposed Experiment

We plan to perform an inclusive measurement at forward angle of the proton spin-dependent cross sections in order to determine the g_2^p structure function in the resonance region for $0.27 < Q^2 < 3.6$ GeV^2. The kinematic coverage, shown in Fig. 8, complements recently published experiment EG4 [14] and will fill in a significant hole in world data for transversely polarized protons. The data is focused in the unmeasured region between the RSS [7] and g2p [3] experiments, but at the recommendation of several senior scientists, is extended with several data points in the high Q^2 regime around 3 GeV^2. This high Q^2 data will help to further investigate the interesting result of the SANE experiment [16] discussed in the previous section. All settings will measure data with a transversely polarized target following the procedures that proved successful during the g2p [3] experiment. Due to the need for very small scattering angles at a beam energy of 4.4 GeV, and a larger central momentum at a beam energy of 8.8 GeV, data will be taken only with the SHMS. Kinematic details are listed in Table 3.

This experiment will require the baseline Hall C equipment, with the addition of a polarized target and chicane magnets.

In Hall C we will require the following technical support from JLab:

1. Installation of the target group's 5T polarized target.

2. Installation of an upstream chicane and associated support structures, or appropriate configuration of the existing 2cm chicane as described in [4].

3. Installation of the slow raster.

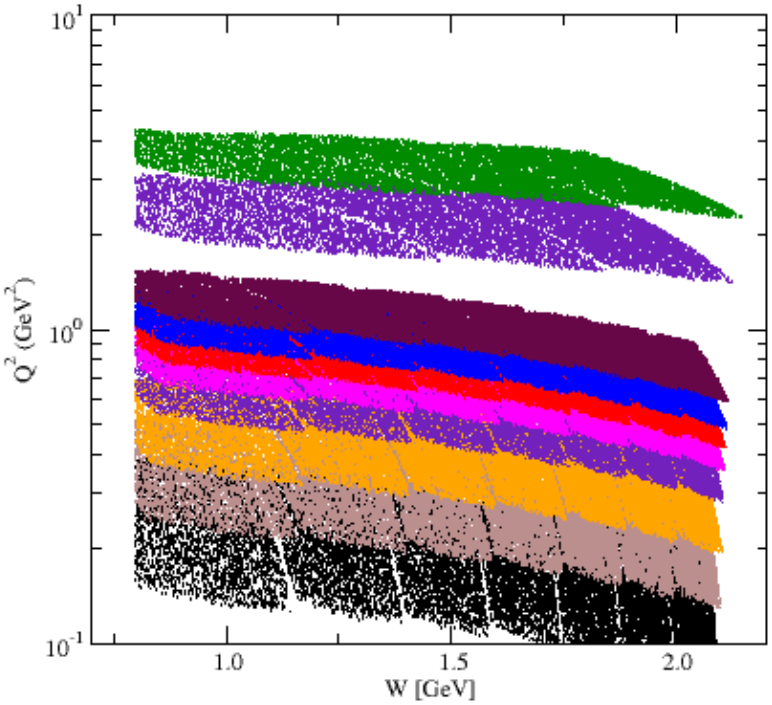

Figure 8: Kinematic coverage for the experiment proposed in this document. Specific beam energies and angles are detailed in Table 3. The black, beige, orange, indigo, magenta, red, blue, and mauve bands represent the 4.4 GeV data, from smallest scattering angle to largest. The violet and green bands represent the 8.8 GeV data, from smallest scattering angle to largest.

4. Operation of the beamline instrumentation for 50-100 nA beam.

We examine these requirements in detail in the following sections since they are not part of the standard setup.

4.1 Polarized Target

The polarized target has been successfully used in many experiments at Jefferson Lab, among the most recent are E01-006, E08-027, and E07-003. This target operates on the principle of Dynamic Nuclear Polarization, to enhance the low temperature (1 K), high magnetic field (5 T) polarization of solid materials (ammonia, lithium hydrides) by microwave pumping. The polarized target assembly contains several target cells of variable length (0.5-3.0 cm) that can be selected individually by remote control to be located in the uniform field region of a superconducting Helmholtz pair. The permeable target cells are immersed in a vessel filled with liquid Helium and maintained at 1 K by use of a high power evaporation refrigerator.

The target material is exposed to ≈140 GHz microwaves to drive the hyperfine transition which aligns the nucleon spins. The DNP technique produces proton polarizations of up to 90% in the NH_3 target. The heating of the target by the beam causes a drop of a few percent in the polarization, and the polarization slowly decreases with time due to radiation damage. Most of the radiation damage can be repaired by annealing the target at about 80 K, until the accumulated dose reached is greater than about 17×10^{15} e^-/cm^2, at which time the target material needs to be replaced. The luminosity of the polarized material in the uniform field region is approximately 85×10^{33} cm^{-2} Hz.

The target will be operated with a magnetic field 90 degrees perpendicular to the beam at all times, to focus the collected data on $\sigma_\perp$.

4.2 Chicane

To access g_2^p, the polarization direction will be held perpendicular to the beam axis for the majority of the experiment. This will create a non-negligible deflection of low energy electrons, so to ensure proper transport of the beam, a chicane will be employed. The first dipole will be located upstream of the target and gives the beam a kick out of the horizontal plane. The second dipole will be need to be mounted on a stand with adjustable height over a range of around 85 cm, and is used to bend the beam back on the target with the required angle to compensate for the 5 Tesla field. Beam Position Monitors (BPMs) will be placed along the chicane line before and after each magnet to ensure proper transport of the beam. The deflection angles created by the 5T target field should be around 2.9 and 1.4 degrees for the 4.4 GeV and 8.8 GeV beam energies respectively.

According to a technical note written by Jay Benesch [4], it is likely that the existing 2 cm vertical chicane in Hall C will suffice for the bending required in this experiment. This should greatly minimize the installation work needed to perform the experiment. According to this technical note, the expected deflection from the center of the target should be on the order of 3mm or less for the beam energies requested, which should be an acceptable deflection given the 1 cm slow raster pattern listed below (Figure 9). Bending from the chicane will likely necessitate the use of a local beam dump, as described below.

4.3 Raster

The existing Hall C fast raster will be used to generate a pattern up to 1 mm x 1 mm and will remain in its standard location [55]. The slow raster will be located approximately 10-12 meters upstream of the target, and can increase the final size up to a circular pattern with a 1 cm radius for 11 GeV [56], with a larger

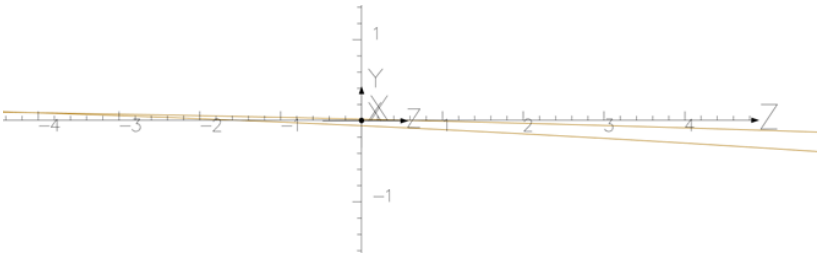

Figure 9: The two beams at the center of the magnet. Vertical span less than 3 mm over 8 cm

viable area for the requested energies of 8.8 and 4.4 GeV. The slow raster is necessary both for the large solid ammonia target that will be required, and to help mitigate the destruction of polarization by the beam discussed above.

4.4 Exit beam pipe and beam dump

The low currents employed in this experiment allow for the use of a simple beam dump constructed by stacking shielding blocks downstream of the target [56]. These blocks can be easily moved with the crane.The connection from the vacuum chamber to the exit beam pipe will need to be modified to accommodate the vertical deflection of the beam, and the coupling to the beam pipe going to the beam dump. A two inch beam pipe is sufficient to accommodate the rastered beam and expected multiple scattering. It is also expected that a beam pipe extension will be necessary due to requiring the smallest angles available to the SHMS detector [55]

4.5 Beamline Instrumentation

4.5.1 Beam Current and Beam Charge Monitor

Beam currents less than 100 nA are typically used with the polarized target in order to limit depolarizing effects and large variations in the density. Standard Beam Current Monitor(BCM) cavities have a linearity good to 0.2% for currents ranging from 180 down to 2 uA. Though it is possible that it will require further time to fully study the linearity, it is likely that the BCMs will remain linear down to 50 nA with the gain on BCM 1 and 2 switched to the highest setting [57].

4.5.2 Beam Polarimetry

We will utilize the Møller polarimeter as part of the standard Hall C equipment. During operation, 0.3 to 0.5 μA of current are incident on a foil of iron polarized by a magnetic field [55]. The expected systematic uncertainty [58, 56] of the Møller measurement is 2% or better. Møller runs will be scheduled at least once per energy change, and will be performed with the (non-chicaned) beam passing to the standard hall C dump.

The Compton polarimeter normally is used for a continuous non-invasive beam polarization monitor. However, it is not very well suited to run at low current, so the primary method of measuring the beam polarization will be with the Møller polarimeter.

4.6 The Spectrometers

4.6.1 Detector Stack

The standard detector stack will be used for detecting electrons. We will require the usual horizontal drift chambers, hodoscope, the gas Cerenkov and lead glass shower calorimeter for particle identification. Since this is an inclusive measurement aiming only to measure scattered electrons, we will not require use of the Aerogel detector.

For this experiment we will use only the SHMS detector, as the HMS detector is inappropriate at many of the scattering angles and energies requested. Performance of the spectrometers are well known so we can expect similar accuracies as for the GDH experiments on the polarized He3 target E94-010 and E97-110.

4.6.2 Optics

It is likely that the optics changes introduced will be very similar to the previous polarized target experiments in Hall C such as SANE[16] and RSS[7]. According to Dave Gaskell[56], the optics changes are likely to be similar to what was seen for previous Hall C polarized target experiments. It has been previously possible to use the standard spectrometer optics in combination with a polarized target field map, and an iterative procedure to correct for the deflection. To verify the optics are well understood, we will plan to take sieve slit data at each setting as a sanity check.

4.6.3 Data Acquisition

We will utilize the standard Hall C data acquisition (DAQ) system which is based on CAEN V1190A TDC and FADC250 ADC. It is expected that the maximum allowed DAQ rate will be at least 20 kHz[59], but is currently being upgraded to a limit of around 40 kHz or more. The calculated rates are on the order of 40 KHz or less, as seen in Table 3. It is therefore unlikely for us to be rate-limited or require a prescale factor.

5 Analysis Method

5.1 Extraction of the g_2 Structure Function

We will perform a polarized cross section measurement in order to determine the spin structure function g_2^p. The spin structure functions are related to the spin-dependent cross sections via:

$$\begin{aligned} g_1 &= \frac{MQ^2}{4\alpha_e^2}\frac{y}{(1-y)(2-y)}\left[\Delta\sigma_{\parallel} + \tan\frac{\theta}{2}\Delta\sigma_{\perp}\right] \\ g_2 &= \frac{MQ^2}{4\alpha_e^2}\frac{y^2}{2(1-y)(2-y)}\left[-\Delta\sigma_{\parallel} + \frac{1+(1-y)\cos\theta}{(1-y)\sin\theta}\Delta\sigma_{\perp}\right] \end{aligned} \tag{22}$$

where $y = \nu/E$.

Here, the polarized cross section differences are represented by $\Delta\sigma_{\parallel}$ and $\Delta\sigma_{\perp}$. Measuring polarized cross section differences results in the cancellation of the contribution from any unpolarized target material and obviates the need for any external model input.

We can recast Eq. 22 in the form:

$$\begin{aligned} g_1 &= K_1(a_1\Delta\sigma_{\parallel} + b_1\Delta\sigma_{\perp}) \\ g_2 &= K_2(c_1\Delta\sigma_{\parallel} + d_1\Delta\sigma_{\perp}) \end{aligned} \tag{23}$$

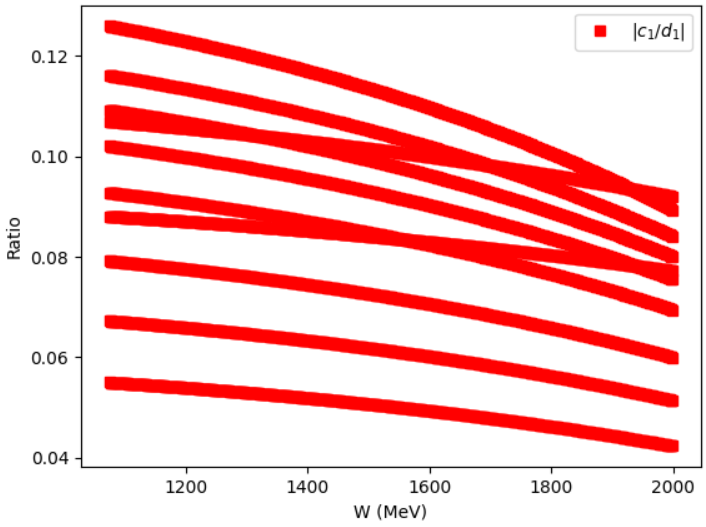

Figure 10: Relative weighting of the $\Delta\sigma_{\parallel}$ contribution to g_2. See Eq. 23.

where

$$
\begin{aligned}
K_1 &= \frac{MQ^2}{4\alpha_e^2}\frac{y}{(1-y)(2-y)} \\
K_2 &= \frac{MQ^2}{4\alpha_e^2}\frac{y^2}{2(1-y)(2-y)} = K_1\frac{y}{2} \\
a_1 &= 1 \\
b_1 &= \tan\frac{\theta}{2} \\
c_1 &= -1 \\
d_1 &= \frac{1+(1-y)\cos\theta}{(1-y)\sin\theta}
\end{aligned}
$$

Equation 23 reveals that the parallel contribution to g_2 is highly suppressed (See Fig. 10). In fact, the relative weight of the $\Delta\sigma_{\parallel}$ contribution to g_2 ranges from 2 to 12% for all proposed kinematics. Since our proposed experiment will not measure $\Delta\sigma_{\parallel}$, we will use the high precision data from Hall B experiments EG4 [60] and EG1b [11], which reported an average uncertainty of approximately 10%. Given the ratio of $|c_1/d_1|$ shown in Figure 23, this leads to around a 2% or less error contribution to our g_2 for all kinematics.

In practice, the Hall B cross section data is not at the exact same kinematics as our proposal, which makes it difficult to directly combine the respective cross sections. Instead, we will use the EG4 and EG1b g_1 data, which has been shown in the previous analysis of E08-027 to be easily adjusted to nearby constant Q^2 with minimal impact on the central value of the structure function [3]. Inverting Eq. 22 yields:

$$
\Delta\sigma_{\parallel} = \frac{4\alpha_e^2}{MQ^2}\frac{(1-y)(2-y)}{y}\left(\frac{2}{y}\right)\frac{\frac{1+(1-y)\cos\theta}{(1-y)\sin\theta}\frac{y}{2}\,g_1 - \tan\theta/2\,g_2}{\frac{1+(1-y)\cos\theta}{(1-y)\sin\theta} + \tan\theta/2}
$$

$$\Delta\sigma_\perp = \frac{4\alpha_e^2}{MQ^2}\frac{(1-y)(2-y)}{y}\left(\frac{2}{y}\right)\frac{\frac{2}{y}g_1+g_2}{\frac{1+(1-y)\cos\theta}{(1-y)\sin\theta}+\tan\theta/2} \quad (24)$$

Eq. 24 can be recast in the form:

$$\Delta\sigma_\parallel = K_3(a_2 g_1 + b_2 g_2) \quad (25)$$
$$\Delta\sigma_\perp = K_4(c_2 g_1 + d_2 g_2) \quad (26)$$

where

$$\begin{aligned}
K_3 &= \frac{4\alpha_e^2}{MQ^2}\frac{(1-y)(2-y)}{y}\left(\frac{2}{y}\right)\frac{1}{a_2-b_2}\\
K_4 &= \frac{4\alpha_e^2}{MQ^2}\frac{(1-y)(2-y)}{y}\left(\frac{2}{y}\right)\frac{1}{a_2-b_2}\\
a_2 &= \frac{1+(1-y)\cos\theta}{(1-y)\sin\theta}\frac{y}{2}\\
b_2 &= -\tan\theta/2\\
c_2 &= \frac{2}{y}\\
d_2 &= 1
\end{aligned}$$

So in terms of the existing Hall B g_1 and the measured $\Delta\sigma_\perp$, g_2 can be expressed:

$$g_2 = \left(\frac{1}{1-K_2K_3c_1b_2}\right)\ [d_1\Delta\sigma_\perp + K_2K_3c_1a_2\ g_1] \quad (27)$$

5.2 Interpolation to Constant Q^2

The data measured at constant incident energy and scattering angle will be interpolated[†] to constant Q^2 as shown in Fig. 8. The good kinematic coverage and overlap should facilitate a straight forward interpolation. It was shown in E08-027 [3] that this method works well when driven by the Hall B Model [11]. The method is performed by comparing additively the model-generated structure function at the constant Q^2 of the setting, usually chosen to be the Q^2 of the $\Delta(1232)$ resonance, and the changing Q^2 of the data to generate a scaling factor. This scaling factor has been shown at the kinematics of E08-027 to contribute only small adjustments to the structure function.

5.3 Systematic Uncertainties

Several JLab experiments have performed measurements similar to what we propose here (for example, see Refs. [6, 7, 13, 14, 16, 3]). From these previous endeavors, we can make an estimate of the systematic uncertainty. Table 1 gives an estimate of the most significant sources of error, while Table 2 gives further detail on the contributions to the cross section uncertainty which will be the dominant error. Previous experience with similar measurements [6] has shown that we can obtain 4-5% systematic uncertainty [61, 62, 63] on cross section measurements, with the largest uncertainty (2-3%) coming from the knowledge of the acceptance.

[†]as has been done in experiments E08027,E94010, E97110 and E01012.

Source	(%)
Cross section	5-7
Target Polarization	3.0
Beam Polarization	3.0
Radiative Corrections	3.0
Parallel Contribution	2.0
Const. Q^2 Adjustment	≤ 1
Total	7.5-8.9

Table 1: Total Systematic Uncertainties.

Source	(%)
Acceptance	4-6
Packing fraction	3.0
Charge determination	1.0
VDC efficiency	1.0
PID detector efficiencies	$\leq$1
Software cut efficiency	$\leq$1
Energy	0.5
Deadtime	$\leq$1
Total	5-7

Table 2: Major contributions to the cross section systematic of Table 1.

A 7.5%[‡] systematic uncertainty on the moments is assumed in Figs. 11 to 13 of section 6.2. Eq. 17 reveals that the unmeasured low-x contribution to $\overline{d_2}$ is suppressed as x^2. In fact, over 90% of the total integral strength (as predicted from the MAID model) is covered in the range from pion threshold to $W = 1.7$ GeV for each of our incident energies. For Γ_2 and I_{LT}, the low-x contribution is poorly understood, but treatments using the Wandzura Wilczek g2 $g2_{WW}$ may be usable over a portion of our proposed kinematic range.

6 Rates and Beam Time Request

The count rate of scattered electrons from the polarized target is given by:

$$\dot{N} = \frac{\mathcal{L}\Delta\Omega\Delta E'\sigma}{f} \tag{28}$$

where $\mathcal{L}$ is the luminosity, $\Delta\Omega$ is the angular acceptance, $\Delta E'$ is the momentum bite, σ represents the proton cross section, and f is the dilution factor which accounts for scattering from unpolarized nucleons in the target.

[‡]relative to the MAID model prediction.

We estimate the experimental cross section by combining proton, nitrogen and helium cross sections from the quasifree scattering model QFS [64]. Inelastic and elastic radiative effects are also included. Table 6 shows the assumed material thickness for a 3 cm target.

The time needed for a given uncertainty δA is given by:

$$T = \frac{1}{\dot{N}(fP_bP_T\delta A)^2} \tag{29}$$

The relevant statistical uncertainty is for the asymmetry, even though this is a cross section measurement, because in the product σA the dominant error arises from A.

The running time and spectrometer configurations are summarized in Table 3. The sixth column represents the rate (in each bin) from the proton, while the seventh shows the total prescaled rate seen by the spectrometer. We assume that the DAQ limit is at least 40 kHz[59]. Initial calculations of the rates are generally far below this limit, eliminating the need for a prescale factor.

Time requested is chosen to bring the statistical error on the moments to the 5-8% range. In general, given the high rate at lower Q^2, this precision can be obtained quickly for many of the settings, but will require more PAC days for the highest kinematics requested.

The choice of parameters used in our rate calculation is summarized in Table 6. We assume an angular acceptance of 5.4 msr and a momentum acceptance of $-10\% < dp < +22\%$, and beam and target polarizations of 80 and 75% respectively. We note that higher polarization values are routinely achieved. Finally, we assume that the minimum time that we would reasonably spend at each setting is one half hour, regardless of how high the rate is.

6.1 Overhead

The incident beam causes radiation damage in the frozen ammonia, which leads to the creation [**?**, **?**] of atomic hydrogen in the target material. This provides an additional relaxation path for the nuclear spins, and the buildup of these free radicals leads to a gradual decay of the target polarization. The concentration of these unwanted radicals can be reduced significantly by raising the temperature of the target to 80-90K, in a process known as annealing. Given the proposed beam current and raster size, we expect to require an anneal about once every 14 hours of beam time. The anneal itself typically requires 2.5 hours from start to beam back on target. The target stick holds two ammonia batches. Each batch can absorb approximately $17{\cdot}10^{15}$ e-/cm^2, at which point the material must be replaced. We expect to swap out target inserts about once every 5 days of accumulated (100% efficient) beam, so a maximum of one target swap should be necessary. To replace the stick and calibrate the NMR instrumentation requires about a shift.

One final overhead arising from the target comes from the need for dedicated empty cell and carbon target runs, which are used to determine the granular target packing fraction and dilution factor. These high rate unpolarized runs can be completed in about one half hour, and we plan to perform them for every other momentum setting.

The experiment should only require one pass change, estimated to require 4 hours. Changing the spectrometer momentum settings requires approximately 15 minutes each on average. We will perform one Møller measurement for each beam energy, each of which requires two hours.

The higher Q^2 points may have a significant positron background from pair production which will need to be accounted for, requiring around an hour of data as well as a ramp down and up of the dipole to change the polarity. The changing of the dipole field can be performed in parallel with other overhead tasks such as TEs, but we estimate the overall time at 4 hours per measurement.

The overhead requirement is summarized in Table 4. We note that previous experience has shown that many overhead tasks can be performed in parallel, or scheduled to coincide with non-delivery of beam. In this sense, our overhead estimate should be conservative.

6.2 Projected Results

Figs. 11 to 14 show the projected accuracy we can obtain with the beam time request of Table 3. The systematic error bands on the axes represent the total from Table 1. The projected uncertainties have been evaluated assuming the central values predicted by the MAID model [34].

7 Summary

We request 18 days in order to perform a precision measurement of g_2^p in the transition region using a transversely polarized proton (NH_3) target, together with the SHMS detector. This measurement will require the use of a Slow Raster and Chicane magnets, but relies on techniques which have been tested and proven successful by a number of other experiments.

The experiment will measure polarized transverse asymmetries and unpolarized cross sections for the proton from an ammonia (NH_3) target. These will be used together to form perpendicular polarized cross section differences. These will be combined with world data at the same kinematics for the parallel polarized cross section to construct the structure function g_2.

This measurement will address a sizeable gap in the measured coverage of g_2 for the proton, and with it, produce several valuable moments which can assist in testing theoretical predictions such as current and future predictions of Lattice QCD.

Among others, the data can be used to study the changing sign of the resonance part of the B.C. sum rule Γ_2 and investigate the implications of a potential sign change in the $\Delta(1232)$ resonance. The data will also further probe the wide variation in JLab d_2 results, and further investigate the interesting result produced by the SANE experiment. The results will also provide data useful for constructing the hyperfine integral Δ_2, which requires measurements of g_2 across a broad spectrum of Q^2 up to 1.1 GeV^2.

This proposal aims to take advantage of an opportunity to measure an important quantity in a region which can be much more easily accessed experimentally than many of its predecessors. This region is ripe with opportunity for further understanding the transition region of QCD, and comparison with upcoming proposals of Lattice QCD. For a comparatively small experimental cost, we will obtain a high precision test of a number of different facets of QCD.

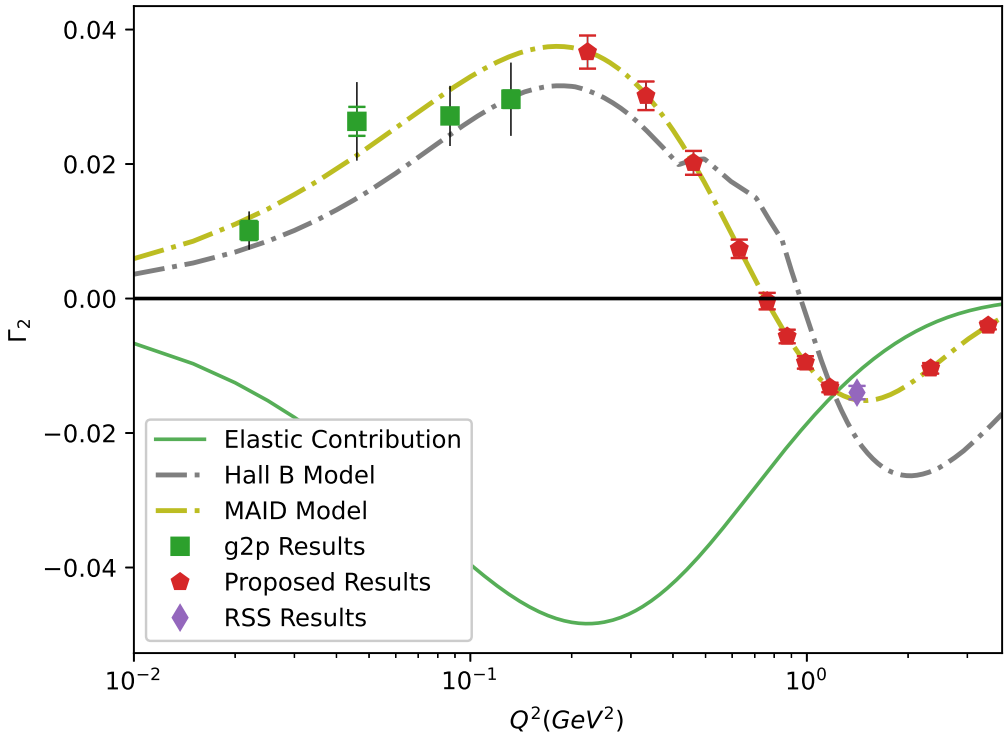

Figure 11: Projected results for Γ_2^p. Data shown is estimated over the resonance region. Statistical errors are shown on the symbols. Systematic for measured region is represented by the light band. Uncertainties for the measured region are evaluated assuming the central value predicted by the MAID [34] model. Elastic curve is from Ref. [65].

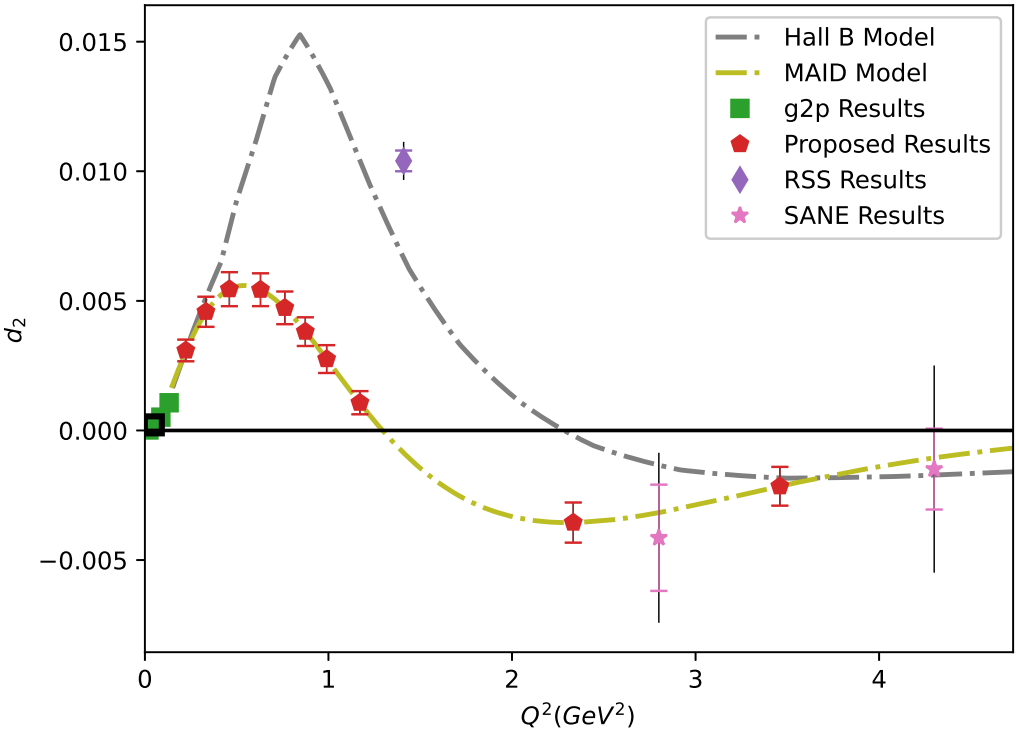

Figure 12: Projected results for d_2^p. Statistical errors are shown on the symbols. Systematic is represented by the band on the axis. Uncertainties are evaluated assuming the central value predicted by the MAID [34] model. The inner (outer) band represents statistical (systematic) uncertainty. Unmeasured non-resonance contribution is highly suppressed by x^2 weighting of d_2 and is not shown.

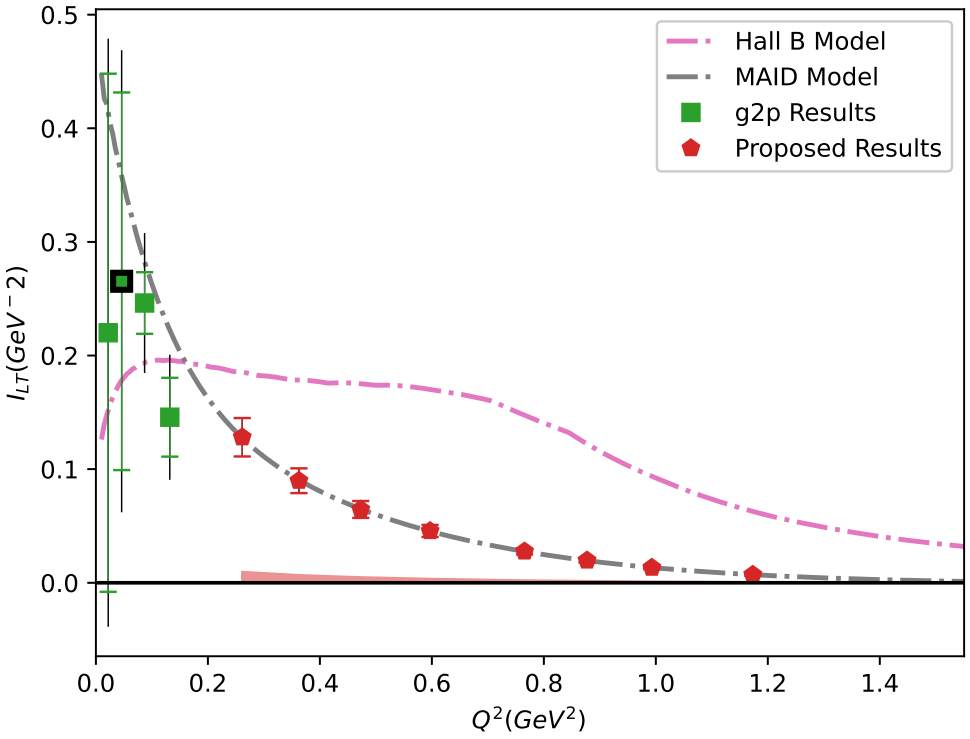

Figure 13: Projected results for I_{LT}. Statistical errors are shown on the symbols. Systematic is represented by the band on the axis. Uncertainties are evaluated assuming the central value predicted by the MAID [34] model.

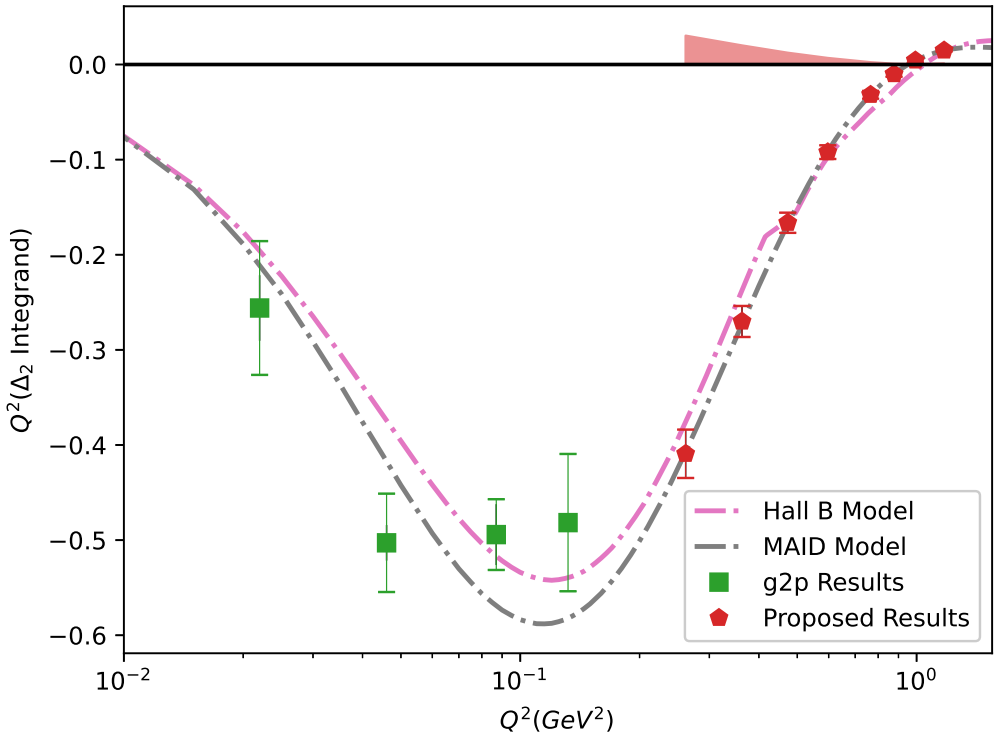

Figure 14: Projected results for the Δ_2 hyperfine structure contribution for muonic hydrogen. Statistical errors are shown on the symbols. Systematic is represented by the band on the axis. Uncertainties are evaluated assuming the central value predicted by the MAID [34] model.

A Beam Time Request Tables

In this section we detail the proposed kinematics and beam time request. In Table 3, all energies and momenta are in GeV, while the luminosity is given in $(\text{cm}^2\text{-s})^{-1}$.

Table 4 summarizes the expected overhead, which was discussed in section 6.1. The expected statistical error is given in Table 5. Table 3 specifies whether we will measure data in the perpendicular configuration alone, or in both perpendicular and parallel configuration for each kinematic. Finally, for reference, in Table 6 we list the relevent experimental parameters that we have assumed in the rate calculation.

Table 3: Beam Time Request.

E_0 (GeV)	Θ (deg)	P_0 (GeV)	W (GeV)	Q^2 (GeV^2)	Rate P (Hz)	Rate (kHz)	Prescale	$\mathcal{L}$	$P_b P_t$	I (nA)	Time (h)
4.4	6.5	3.607	1.47	0.204	77	40.0	1	0.9E+35	0.60	85	1.0
4.4	6.5	2.661	2.00	0.151	65	25.1	1	0.9E+35	0.60	85	1.0
4.4	6.5	1.963	2.31	0.111	69	18.9	1	0.9E+35	0.60	85	1.0
										0.1	PAC days
4.4	8.0	3.607	1.44	0.309	41	21.4	1	0.9E+35	0.56	85	1.3
4.4	8.0	2.661	1.98	0.228	28	11.5	1	0.9E+35	0.56	85	1.9
4.4	8.0	1.963	2.30	0.168	30	8.3	1	0.9E+35	0.56	85	1.8
										0.2	PAC days
4.4	9.5	3.607	1.39	0.435	18	9.1	1	0.9E+35	0.60	85	2.3
4.4	9.5	2.661	1.96	0.321	14	5.9	1	0.9E+35	0.60	85	3.0
4.4	9.5	1.963	2.28	0.237	15	4.3	1	0.9E+35	0.60	85	2.8
										0.3	PAC days
4.4	11.2	3.607	1.33	0.610	7	3.7	1	0.9E+35	0.56	85	6.0
4.4	11.2	2.661	1.92	0.450	6	3.0	1	0.9E+35	0.56	85	6.5
4.4	11.2	1.963	2.26	0.332	7	2.2	1	0.9E+35	0.56	85	5.9
										0.8	PAC days
4.4	12.5	3.607	1.27	0.752	4	2.0	1	0.9E+35	0.57	85	9.1
4.4	12.5	2.661	1.89	0.555	4	1.9	1	0.9E+35	0.57	85	8.5
4.4	12.5	1.963	2.25	0.409	4	1.5	1	0.9E+35	0.57	85	7.6
										1.1	PAC days
4.4	13.5	3.607	1.22	0.877	2	1.3	1	0.9E+35	0.56	85	16.5
4.4	13.5	2.661	1.87	0.647	3	1.3	1	0.9E+35	0.56	85	13.7
4.4	13.5	1.963	2.23	0.477	3	1.1	1	0.9E+35	0.56	85	12.1
										1.8	PAC days
4.4	14.5	3.607	1.17	1.011	1	0.8	1	0.9E+35	0.56	85	23.2
4.4	14.5	2.661	1.84	0.746	2	1.0	1	0.9E+35	0.56	85	17.4
4.4	14.5	1.963	2.21	0.550	2	0.8	1	0.9E+35	0.56	85	14.9
										2.3	PAC days
4.4	16.0	3.607	1.07	1.229	0	0.4	1	0.9E+35	0.56	85	50.8
4.4	16.0	2.661	1.80	0.907	1	0.6	1	0.9E+35	0.56	85	32.7
4.4	16.0	1.963	2.19	0.669	1	0.5	1	0.9E+35	0.56	85	26.6
										4.6	PAC days
8.8	11.0	7.213	1.24	2.332	0	0.5	1	0.9E+35	0.56	85	33.3
8.8	11.0	5.321	2.38	1.721	0	0.8	1	0.9E+35	0.56	85	19.0
										2.2	PAC days
8.8	14.0	7.213	0.30	3.771	0	0.1	1	0.9E+35	0.56	85	101.8
8.8	14.0	5.321	2.15	2.782	0	0.2	1	0.9E+35	0.56	85	31.6
										5.6	PAC days

Parameter	Value
$\Delta\Omega$ [msr]	5.4
$\pm\delta P[\%]$	16.0
T_b	0.032
T_a	0.032
Minimum time per setting [hr]	1.0
Minimum Momentum [MeV]	500.0
Maximum Momentum (L) [MeV]	9000.0
Maximum Momentum (R) [MeV]	9000.0
Daq Limit [kHz]	40.0
Packing Fraction	0.55

Table 6: Experiment Parameters

Table 4: Overhead

Overhead	Number	Time Per (hr)	(hr)
Target anneal	45	2.5	112.5
–Beamline survey	10	8.0	80.0
Target swap	2	8.0	16.0
Target T.E.	4	2.0	8.0
Target field ramp	10	1.0	10.0
Dilution	28	0.50	14.0
Pass change	2	4.0	8.0
Momentum change	28	0.50	14.0
Moller measurement	10	2.0	20.0
Pair-symmetric background measurement	2	4.0	8.0
Optics/elastic calibration	2	16.0	32.0
BCM calibration	2	4.0	8.0
			344.5

Table 5: Statistical Uncertainty

Kinematic	$A_{\parallel}$ error	$A_{\perp}$ error
1	0.012	0.010
2	0.013	0.011
3	0.014	0.012
4	0.015	0.012
5	0.016	0.013
6	0.017	0.012
7	0.017	0.013
8	0.016	0.012
9	0.016	0.021
10	0.016	0.032

* EG4 expected uncertainty.

References

[1] Nuclear Physics Comparative Research Review for the U. S. Department of Energy, Oct 2013. http://science.energy.gov/np/news-and-resources.

[2] W. Armstrong et al. Revealing color forces with transverse polarized electron scattering. *Phys. Rev. Lett.*, 122:022002, Jan 2019.

[3] D. Ruth, R. Zielinski, C. Gu, et al. Proton spin structure and generalized polarizabilities in the strong quantum chromodynamics regime. *Nature Physics*, 2022.

[4] J. Benesch. Examination of the need for an upstream chicane for proposal "A Measurement of the Proton g2 Structure Function at Intermediate Q2". Technical report, 2023.

[5] 2023 low-q workshop. Chania, Greece.

[6] M. Amarian et al. Measurement of the Generalized Forward Spin Polarizabilities of the Neutron. *Phys. Rev. Lett.*, 93:152301, 2004.

[7] F. R. Wesselmann, K. Slifer, S. Tajima, et al. Proton Spin Structure in the Resonance Region. *Phys. Rev. Lett.*, 98:132003, 2007.

[8] R. Fatemi *et al. Phys. Rev. Lett.*, 91, 2003.

[9] J. Yun *et al. Phys. Rev. C*, 67, 2003.

[10] A. Deur *et al. Phys. Rev. Lett.*, 93, 2004.

[11] Y. Prok, P. Bosted, V.D. Burkert, A. Deur, K.V. Dharmawardane, G.E. Dodge, K.A. Griffioen, S.E. Kuhn, R. Minehart, et al. Moments of the spin structure functions and for g_1^p and g_1^d for $0.05 < Q^2 < 3.0$ GeV^2. *Physics Letters B*, 672(1):12 – 16, 2009.

[12] J. P. Chen. Moments of Spin Structure Functions: Sum Rules and Polarizabilities. *Int. J. Mod. Phys.*, E19:1893–1921, 2010.

[13] F. Garibaldi spokespersons. J. P. Chen, A. Deur. Jlab experiment e97-110.

[14] M. Battaglieri, R. De Vita, A. Deur, M. Ripani, et al. Jefferson Lab CLAS EG4 Run Group. http://www.jlab.org/expprog/proposals/03/PR03-006.pdf.

[15] S. Choi J. P. Chen and spokespersons. N. Liyanage. Jlab experiment e01-012.

[16] O. A. Rondon. The RSS and SANE Experiments at Jefferson Lab. *AIP Conference Proceedings*, 1155(1):82–92, 2009.

[17] C. G. Callan and David J. Gross. High-energy electroproduction and the constitution of the electric current. *Phys. Rev. Lett.*, 22:156–159, Jan 1969.

[18] R. L. Jaffe. G(2): The Nucleon's Other Spin Dependent Structure Function. *Comments Nucl. Part. Phys.*, 19:239, 1990.

[19] S. Wandzura and Frank Wilczek. Sum rules for spin dependent electroproduction: Test of relativistic constituent quarks. *Phys. Lett.*, B72:195, 1977.

[20] S. D. Drell and A. C. Hearn. Exact Sum Rule for Nucleon Magnetic Moments. *Phys. Rev. Lett.*, 16:908–911, 1966.

[21] D. Drechsel, S. S. Kamalov, and L. Tiator. Gerasimov-Drell-Hearn Sum Rule and Related Integrals. *Phys. Rev. D*, 63:114010, 2001.

[22] Xiang-Dong Ji and Jonathan Osborne. Generalized sum rules for spin-dependent structure functions of the nucleon. *J. Phys.*, G27:127, 2001.

[23] D. Drechsel, B. Pasquini, and M. Vanderhaeghen. Dispersion Relations in Real and Virtual Compton Scattering. *Phys. Rept.*, 378:99–205, 2003.

[24] V. Lensky, J. M. Alarcón, and V. Pascalutsa. Moments of Nucleon Structure Functions at Next–To–Leading Order in Baryon Chiral Perturbation Theory. *Phys. Rev. C*, 90:055202, Nov 2014.

[25] R. L. Jaffe and X.-D. Ji. Studies of the Transverse Spin-Dependent Structure Function $g_2(x, Q^2)$. *Phys. Rev. D*, 43:724–732, 1991.

[26] Aneesh V. Manohar. An introduction to spin dependent deep inelastic scattering, 1992.

[27] Robert L. Jaffe. Spin, twist and hadron structure in deep inelastic processes. 1996.

[28] J. Soffer and O. Teryaev. QCD Radiative and Power Corrections and Generalized Gerasimov-Drell-Hearn Sum Rules. *Phys. Rev. D*, 70:116004, 2004.

[29] Z. E. Meziani et al. Higher twists and color polarizabilities in the neutron. *Phys. Lett.*, B613:148–153, 2005.

[30] Aldo Antognini, Franziska Hagelstein, and Vladimir Pascalutsa. The Proton Structure in and out of Muonic Hydrogen. *Annual Review of Nuclear and Particle Science*, 72:389–418, September 2022.

[31] P. L. Anthony et al. Precision measurement of the proton and deuteron spin structure functions g2 and asymmetries a(2). *Phys. Lett.*, B553:18–24, 2003.

[32] S. Simula, M. Osipenko, G. Ricco, and M. Taiuti. Leading and higher twists in the proton polarized structure function g1(p) at large Bjorken x. *Phys. Rev.*, D65:034017, 2002.

[33] Robert Fersch et al. Determination of the Proton Spin Structure Functions for $0.05 < Q^2 < 5$ GeV^2 using CLAS. *Phys. Rev. C*, 96:065208, Dec 2017.

[34] D. Drechsel, S. S. Kamalov, and L. Tiator. Unitary Isobar Model – MAID2007. *The European Physical Journal A*, 34(1):69, 2007.

[35] M. Stratmann, Z. Phys. C **60**, 763 (1993).

[36] X. Song, Phys. Rev. D **54**, 1955 (1996).

[37] H. Weigel and L. Gamberg, Nucl. Phys. A **680**, 48 (2000);.

[38] M. Wakamatsu, Phys. Lett. B **487**, 118 (2000).

[39] P.L. Anthony et al. Precision Measurement of the Proton and Deuteron Spin Structure Functions g_2 and Asymmetries A_2. *Physics Letters B*, 553(1–2):18 – 24, 2003.

[40] P.L. Anthony et al. Measurement of the Proton and Deuteron Spin Structure Functions g_2 and Asymmetry A_2. *Physics Letters B*, 458(4):529 – 535, 1999.

[41] D. Flay et al. Measurements of d_2^n and A_1^n: Probing the neutron spin structure. *Phys. Rev. D*, 94:052003, Sep 2016.

[42] M. Gockeler, R. Horsley, W. Kurzinger, H. Oelrich, D. Pleiter, Paul E. L. Rakow, A. Schafer, and G. Schierholz. A Lattice calculation of the nucleon's spin dependent structure function g(2) revisited. *Phys. Rev. D*, 63:074506, 2001.

[43] F. R. Wesselmann et al. Proton Spin Structure in the Resonance Region. *Phys. Rev. Lett.*, 98:132003, 2007.

[44] K. Slifer et al. 3He Spin-Dependent Cross Sections and Sum Rules. *Phys. Rev. Lett.*, 101:022303, 2008.

[45] I.I. Balitsky, V.M. Braun, and A.V. Kolesnichenko. Power corrections 1/q2to parton sum rules for deep inelastic scattering from polarized nucleons. *Physics Letters B*, 242(2):245–250, 1990.

[46] A.I. Signal. Calculations of higher twist distribution functions in the MIT bag model. *Nuclear Physics B*, 497(1-2):415–434, jul 1997.

[47] V. M. Braun, T. Lautenschlager, A. N. Manashov, and B. Pirnay. Higher twist parton distributions from light-cone wave functions. *Phys. Rev. D*, 83:094023, May 2011.

[48] M. Osipenko et al. Global analysis of data on the proton structure function g1 and extraction of its moments. *Phys. Rev.*, D71:054007, 2005.

[49] Jose Manuel Alarcón, Franziska Hagelstein, Vadim Lensky, and Vladimir Pascalutsa. Forward doubly-virtual compton scattering off the nucleon in chiral perturbation theory. ii. spin polarizabilities and moments of polarized structure functions. *Phys. Rev. D*, 102:114026, Dec 2020.

[50] V. Olmos de Leon *et al.*, Eur. Phys. J. **A 10**, 207 (2001); J. Tonnison *et al.*, Phys. Rev. Lett. **80**, 4382 (1998).

[51] Mainz Proposal A1/01-00: "Double polarization Virtual Compton Scattering in the threshold regime". http://wwwa1.kph.uni-mainz.de/A1/publications/ proposals/.

[52] J. Ahrens *et al.*, Phys. Rev. Lett. **87**, 022003 (2001).

[53] V. Bernard, E. Epelbaum, and U.-G. Krebs, H.and Meissner. New Insights into the Spin Structure of the Nucleon. *Phys. Rev. D*, 87:054032, 2013.

[54] C.-W. Kao, T. Spitzenberg, and M. Vanderhaeghen. Burkhardt-Cottingham Sum Rule and Forward Spin Polarizabilities in Heavy Baryon Chiral Perturbation Theory. *Phys. Rev. D*, 67:016001, 2003.

[55] Hall C Standard Equipment Manual 2019. `https://hallcweb.jlab.org/safety-docs/current/Standard-Equipment-Manual.pdf`.

[56] D. Gaskell. Private conversation.

[57] D. Mack. Private conversation.

[58] J. Alcorn et al. Basic Instrumentation for Hall A at Jefferson Lab. *Nucl. Instrum. Meth.*, A522:294–346, 2004.

[59] D. Camsonne. Private conversation.

[60] X. Zheng, A. Deur, H. Kang, et al. Measurement of the proton spin structure at long distances. *Nature Physics*, 17:736–741, 2021.

[61] K. Slifer, E94010 Technical Note #37 : "Dependence of the Cross-Section on Acceptance Cuts for E94010", (2001).

[62] K. Slifer, E94010 Technical Note #38 : "E94010 Unpolarized ^{3}He Cross Sections", (2001).

[63] K. Slifer, Ph.D. Thesis. Temple University (2004).

[64] J.S. O'Connell and Lightbody J.W. Jr. Modeling Single Arm Electron Scattering and Nucleon Production From Nuclei by GeV Electrons. *Comput. Phys.; (United States)*, 2:3, 1988.

[65] Earle L. Lomon. Effect of recent R(p) and R(n) measurements on extended Gari-Kruempelmann model fits to nucleon electromagnetic form factors. *Phys. Rev.*, C66:045501, 2002.